THE ZWITTERION ISOMER OF ORTHOSILICIC ACID AND ITS ROLE IN NEUTRAL pH DIMERIZATION FROM DENSITY FUNCTIONAL THEORY

Mihali A. Felipe

Molecular Biophysics & Biochemistry
Yale University
New Haven CT 06511 USA
mihali.felipe@yale.edu

ABSTRACT. Using density functional theory, the plausible existence of the zwitterion isomer of orthosilicic acid is proposed to account for some of the properties of silica in water. Explicit hydration and explicit addition of salt are used in modeling the zwitterion and the dimerization reaction. Paths between orthosilicic acid, the zwitterion and the autoionization products are presented. The p*K* for the formation of the aqueous zwitterion species is calculated to be 7.78 in dilute silica solutions and the activation energy for the dimerization reaction ranges from 59.8 kJ/mol to 70.7 kJ/mol depending on salt concentration.

INTRODUCTION

Orthosilicic acid is the most fundamental building block of dissolved silica, which are themselves among the most ubiquitous classes of compounds found in surface waters. A thorough understanding of the chemistry of orthosilicic acid is therefore vital to elucidate phenomena involving silica such as mineralization, nutrient bioavailability, and geothermal well

scaling. Unfortunately, although great effort has been expended in experiments and simulation, the dimerization reaction, which is one of the simplest of its reactions, is still not very well understood; the same can be said about the reverse reaction, or the hydrolysis of the dimer.

Studies on the reaction order are conflicting and indicate that much is not known about the dynamics of silica in solution at the atomic scale. Studies at pH 4 by Alexander and others (1954) showed third order kinetics in agreement with Goto (1956) who conducted work at pH 7 to 10. However, Rothbaum and Rohde (1979) found the oligomerization at pH 7 to 8 to be second order and Icopini and others (2005) reported fourth order rates from pH 3 to 11. Gorrepati and others (2010) found second order rates below pH 0. The activation energies from these studies vary from 12.6 kJ/mol (Rothbaum and Rohde, 1979), to 58 kJ/mol (Harrison and Loton, 1995), to 71 kJ/mol (Makrides and others, 1980).

The dependence of the kinetics on ionic strength, or alternatively cation concentration, is just as puzzling (Rimstidt, 2015). Sodium ion has been shown to decrease the reaction rate of silica condensation at early stages (Harrison and Loton, 1995) yet increase crystallization and growth at later stages (Burkett and Davis, 1995). Icopini and others (2005) found an exponential increase in oligomerization rates with ionic strength. Gorrepatti et al (2010) found rates that varied with the salt added according to the following relationship: $AlCl_3$ > $CaCl_2$ > $MgCl_2$ > NaCl > CsCl > no salt. How these phenomena happen is unresolved. The complex relationships between rates and pH and ionic strength open the question of the existence of yet unidentified reactive species or class of species that favor neutral pH and high ionic strength.

Simulation has been providing immense insight to understanding the dimerization process, aiding in the discovery of species that would not otherwise have been easily identified by

experiment, and allowing the examination of molecular scale local effects. Simulation methods have grown in sophistication in parallel with the development of computing memory and processing power. The primary emphasis in the present study is on density functional theory methods (DFT) specifically, although other schemes that are in active development and application such as molecular dynamics (Iztova et al, 2020; Kirk and others, 2011; Jorge and others, 2009) and Monte Carlo (Martin and others, 2021; Zhang and others, 2012; Malani and others 2010) have also been applied to investigate these mechanism. These other schemes are able to model chemical systems up to the micrometer scale that would not be practicable with DFT. However, the elucidation of chemical reactivity is still principally a question that is best handled on the atomic-length scale by DFT and ab initio methods in general because of the changes in bonding, and therefore electronic structure, during the course of a reaction. At the same time, it is worth noting that there are methods that algorithmically combine the strengths of both ab initio and molecular dynamics aptly named ab initio molecular dynamics (Pavlova and others, 2013; Trinh and others, 2009; Car and Parinello, 1985).

The impetus of these simulations is to model the real system as closely as computationally practical, and to incorporate all physical influences on the reaction center. In this regard, the nascent ab initio work by Xiao and Lasaga (1996, 1994) on acid and base catalyzed hydrolysis of the dimer were attempts to draw silica solution chemistry from dry, gas-phase simulations. Subsequently, the utilization of implicit solvation improved the energy calculations taking into account long range effects that the solvent imparts on the reacting ensemble (Mora-Fonz and Catlow, 2007; Pelmenschikov and others, 1997; Tossel, 2005) without significant computational overhead. However, the explicit addition of water molecules revealed that favorable reaction paths may be starkly different from the dry, gas-phase simulations, even with implicit solvation

included (Trinh and others, 2009; Heenan and others, 2020; Zhang and others, 2017) suggesting that long range interactions have a less influential role on the mechanisms than short range electrostatics and, more specifically, than hydrogen bonding. These effects are predominantly due to the ease of formation of hydrogen bonds by water molecules, which lowers energies significantly (12.6-33.4 kJ/mol, Huš and Urbic, 2012), and the ability of water to form proton wires where hydrogens can concertedly move around and participate in the so-called Grotthus mechanism (van Grotthus, 1806; for example, Liu and others, 2019). Furthermore, the hydroxides of H_4SiO_4 themselves have been shown to participate in mobilizing hydrogen through similar mechanism (Felipe and others, 2004) in aqueous environments.

It is interesting to note that so far studies on the neutral pH dimerization have primarily focused on the reactivity of H_4SiO_4, and in particular on the nucleophilicity of hydroxide oxygens and the electro-positivity of the central silicon. For example, Trinh and others (2006) arrived at a one-step dimerization mechanism where the hydroxide oxygen of one orthosilicic acid attacks the silicon of another directly. However, this mechanism yielded a high activation energy of 127 kJ/mol and the energetics have been corroborated by succeeding simulation studies with only minor modifications (Hu and others, 2013; Liu and others, 2019). Furthermore, it does not explain why there is dependence of the kinetics on the ionic strength. It has increasingly become apparent that this mechanism cannot account for the empirical activation energies observed. These open the possibility of whether the canonical equations of orthosilicic acid speciation in water (Iler, 1979; Rimstidt and Barnes, 1980; Sjöberg and others, 1981), or

$$H_4SiO_4 \leftrightarrow H_3SiO_4^- + H^+ \qquad pK_{a1} = 9.472 \text{ (in 0.6 M NaCl)} \qquad (1)$$

$$H_3SiO_4^- \leftrightarrow H_2SiO_4^{2-} + H^+ \qquad pK_{a2} = 12.650 \text{ (in 0.6 M NaCl)} \qquad (2)$$

92 represent all the relevant species in solution. In particular, some molecules that have appeared in
93 simulations and that were considered reaction intermediates are more energetically stable than
94 the auto-ionization products given by equations (1) and (2). Also, these reaction intermediates
95 are intriguing compounds in themselves from the standpoint of biochemical reactions, as well as
96 their potential uses in industry and manufacturing.

97 The present work aims to accomplish three things. First, a zwitterion form of orthosilicic acid is
98 examined in the neutral pH regime. This zwitterion is derived from similar reaction intermediates
99 reported by Mondal and others (2009) and Zhou and others (2002). Second, its relevance in the
100 dimerization reaction of silica through representative reactions is investigated. Third, the effects
101 of explicitly adding sodium chloride to the system are evaluated. It is therefore envisaged that the
102 dimerization proceeds as depicted in figure 1 and is positively influenced by the ionic strength.

103 METHODOLOGY AND THEORY

104 Density functional theoretical calculations were performed on constructed model systems using
105 the Gaussian 16 suite of programs (Frisch and others, 2016) running in Dell PowerEdge M620
106 servers. The three-parameter hybrid functional B3LYP method was utilized and two types of
107 basis sets were used: one which purely uses 6-311++G(d,p) on all atoms, and another which is a
108 customized combination of 6-311++G(d,p) and 6-31+G(d) on specified atom centers, henceforth
109 designated 6-311++G(d,p)[36]/6-31+G(d), where "[36]" represents the number of atom centers
110 to which 6-311++G(d,p) are applied. The use of the B3LYP method and the 6-311++G(d,p) basis
111 set together is mainly because they are known to produce good estimates of thermochemistry for
112 silicate systems (Cypryk and Gostynski, 2016) and because their use would facilitate the ease of
113 comparison with previous studies (for example, Cheng and others, 2012; Criscenti and others,

114 2006; Alkorta and others, 2001). The use of 6-311++G(d,p)[36]/6-31+G(d) was used for the
115 bigger chemical systems for computing tractability, and is similar to the method that was
116 evaluated by Yang and others (2009).

117 The initial model systems, or configurations of atoms, were prepared as follows:

118 1. The starting configuration of the "pure-water" model simulation was constructed first.
119 Twenty-seven water molecules were added randomly and evenly around an H_4SiO_4 molecule.
120 The resulting system was optimized at 6-31+G(d) and subsequently to the desired level of 6-
121 311++G(d,p).

122 2. Another H_4SiO_4 was added to the system above and thirty-one water molecules were added
123 randomly and evenly around. The resulting system was optimized at 6-31+G(d) and
124 subsequently to the desired level of 6-311++G(d,p)[36]/6-31+G(d). The choice of the thirty-six
125 atoms that made use of the higher 6-311++G(d,p) basis sets was done from defining a reaction
126 center – the set of molecules with the anticipated bond-breaking and bond formation and the
127 immediately neighboring water molecules. This is the starting configuration of the pure-water
128 model for dimerization.

129 3. Atoms of Na and Cl were added to the two systems above, leading to two additional systems.
130 The placements of the two atoms were arbitrary but juxtaposed to each other. These systems
131 were likewise optimized to the respective desired basis sets.

132 The four resulting systems from the procedure described above were clusters of molecules that
133 had 90, 92, 195 and 197 atoms each. Constrained optimizations were performed on the structures
134 to determine other minima and first order saddle-points in between them. Transition state

optimizations were done with the synchronous transit-guided quasi-Newton method at the respective basis sets mentioned above, followed by vibrational frequency calculations to establish that structures are true saddle points. All minima were fully optimized and analyzed for harmonic vibrational frequencies and zero-point energies. Optimization calculations yield stationary points that are internal energy minima along a potential energy surface (PES), which is a hypothetical surface where vibrations are absent. However, even in the ground state, a chemical system would have a ground state energy or zero-point energy. Hence, internal energies need to be corrected and form another surface that is elevated in energy from the PES, or a zero-point energy corrected PES. While the two surfaces might have similar topologies, this may not always be the case particularly in the case of shallow potential energy wells.

Atomic charge distributions were accomplished by Hirshfeld population analysis (Hirshfeld, 1977), and CM5 calculations (Marenich and others, 2012; Wiberg and Rablen, 2018). The more common Mulliken (1955) population analyses results were not reported as it is considered sensitive to basis set size and to the choice of basis (Marenich and others, 2012) and deemed less reliable than either Hirshfeld or CM5.

RESULTS

The computations in this study resulted in a total of eighteen fully optimized energy minima and thirteen associated intervening fully optimized first-order saddle points that connect the paths of the reactions of interest; these are all referred to as “stationary points”. The fully optimized minima represent reactants, products, and intermediates, and the first-order saddle points

represent transition states. These stationary points are in four distinct systems each with their own elemental compositions and assigned basis sets. Relative energy changes were calculated between stationary points along a reaction path within each system only. The complete set of configurations are listed in the supplement. Note that these discovered pathways determine the current best upper bounds to activation energies because competing pathways would need to have reaction rates that are equal to or greater than these mechanisms.

Pure water: H_4SiO_4 + 27H_2O system

There were two species of silica that can be identified in this system through following reaction paths and exploring the PES. As expected from numerous previous DFT and ab initio studies, one of these species is orthosilicic acid. The other species is a zwitterion isomer of orthosilicic acid, which henceforth will be referred to as orthosilicic acid zwitterion ($SiO^-(OH)_2(H_2O)^+$, or OSAZ). Initial configurations representing auto-ionization of the silica to $H_3SiO_4^-$ and free H^+ or H_3O^+ did not stabilize but optimized to either OSAZ or H_4SiO_4.

There are twelve possible tetrahedral arrangements for two –OH groups, one $–O^-$ group and one $–OH_2^+$- group around a silicon atom. For computational practicality therefore, only one of these combinations was arbitrarily chosen for determining the isomer transformation path. An energetically viable path for the transformation between the two minima was determined and is shown in figure 2; the corresponding change in energies for the elementary and net reactions are listed in table 1.

Presented are the internal energy changes (ΔU), the internal energy changes corrected for zero-point energies (ΔU_{zpc}) and the Gibbs free energy changes at 298K (ΔG_{298}). Free energies were

evaluated by frequency calculations at 298.15K and 1 atm. Note that the equilibrium constant K, and pK are related to the ΔG of the net overall reactions by

$$K = - \exp(-\Delta G/\mathrm{R}T) \text{ and} \quad (3)$$

$$\mathrm{p}K = - \log (K) \quad (4)$$

The computed net free energy indicates that the forward reaction from orthosilicic acid to OSAZ is less favored than the reverse reaction.

No stationary points that represent free protons (H^+), hydronium ion (H_3O^+) or dihydroxonium ions ($H_5O_2^+$) were found in the pure water system. While this does not demonstrate non-existence of these local minima, it suggests that if these positively charged aqueous species ever do exist, they may be occurring in very shallow PES wells where configurations can easily evolve to more energetically favorable species such as OSAZ, or the system size constrains the separation of H^+ and H_3SiO4^- preventing the optimization to a stable configuration where they are far apart. In the system size under consideration, it suggests that the pure water case is less conducive to their formation.

Salt-present: H_4SiO_4 + 27H_2O + NaCl system

There were two species of silica that can be identified in this system through following reaction paths and exploring the PES. Again and as expected, orthosilicic acid is one of them. The other species is $H_3SiO_4^-$ that is charge balanced by a hydronium ion (H_3O^+) with a water molecule in between them, denoted by H_3O^+•H_2O•$H_3SiO_4^-$, where the dot • refers to hydrogen bonding. The

196 two hydrogen bonds are from 1.4A to 1.7A in length. This structural configuration would be
197 referred to as "dipolar complex I", from hereon.

198 The reaction path from orthosilicic acid to dipolar complex I was computed. Because there are
199 several possible configurations of $H_3O^+ \bullet H_2O \bullet H_3SiO_4^-$, a representative transformation path from
200 one dipolar complex I configuration to another was computed. The results are shown in figure 3
201 and the corresponding energies are listed in table 1. Attempts to optimize OSAZ to an energy
202 minimum were not successful in this system. Instead, OSAZ-like structures manifest as transition
203 states between different dipolar complex I configurations.

204 To estimate the concentration of NaCl in the system being modeled, gross volume calculations
205 were performed by defining the surface as the contour of 0.001 electrons/Bohr3 density and
206 using a Monte Carlo integration method (Parsons and Ninham, 2009). This method yielded
207 volumes of 490 cc/mole and 460 cc/mole for figure 3C and 3D respectively, corresponding to
208 concentrations of 2.0M and 2.2M of NaCl. In comparison, saturated brine is 6.14M NaCl and
209 seawater is 0.469 moles/kg NaCl (Culkin and Cox, 1966)

210 *Dimerization in pure water: $2H_4SiO_4 + 60H_2O$ system*

211 Four species of silica were identified in this system through following the reaction paths and
212 exploring the PES. Namely, these species are orthosilicic acid, OSAZ, $H_3SiO_4^-$, and $H_6Si_2O_7$.
213 Hence, there are potentially at least six reaction paths that can be explored in this system. The
214 focus however is to find the relevance of OSAZ to the dimerization reaction and to the other
215 three species, and therefore not all reaction paths were investigated. The results are shown in
216 table 2.

217 Table 2A and figure 4 show the possible mechanism to dimerization under neutral pH in pure
218 water. The process begins with two H_4SiO_4 molecules sitting side-by-side. Next, one of the
219 H_4SiO_4 molecules transforms to OSAZ. Subsequently, H-bonding draws the two different silica
220 molecules closer together. Finally, the H_4SiO_4 molecule simultaneously donates a proton,
221 performs a nucleophilic attack on the silicon of OSAZ, and causes the H_2O group of OSAZ to
222 eject.

223 Figure 5 shows the formation of $H_3SiO_4^-$ from OSAZ. Note that the $H_3SiO_4^-$ species is charge
224 balanced by the immediately neighboring H_3O^+ formed from the freed proton (fig. 5E) and will
225 be referred to as "dipolar complex II" from hereon. A second configuration where H_3O^+ is more
226 distant (fig. 5F) but much higher in energy was also found. The energy profiles corresponding to
227 the configurations in figures 4 and 5 are shown in figure 6.

228 Because the bond breaking and bond formation during $H_3SiO_4^-$ production (figs. 6C, 6E, 6F)
229 involve atoms that were not among the thirty-six that were initially assigned the high basis set, a
230 test on the reliability of the results was performed by reassignment of basis sets on atom centers.
231 Optimization and frequency calculations were performed producing a second, generally similar,
232 energy curve (eqs A7 to A10 in table 2) and to nearly identical configuration geometries, based
233 on RMSD of 0.020A-0.028A; here, the RMSD was determined by Kabsch algorithm (Kabsch,
234 1976). Equation (A9) in table 2 was the most sensitive to this reassignment and change in basis,
235 but exhibiting a free energy difference of only 3.1 kJ/mol.

236 Net reactions and thermodynamic quantities are shown in table 3. It should be emphasized that
237 because of the size of the systems used in the models, the thermodynamic quantities listed here
238 do not describe the global thermodynamics of the solution but of the local environment in the

239 vicinity of the reaction zone. The quantities are however useful in comparing the relative
240 favorability of the different molecular configurations where the dimerization reaction is
241 occuring. Note that the free energies indicate that the dimerization reaction (eq A1 in table 3) is
242 thermodynamically favored.

243 *Dimerization with salt present: $2H_4SiO_4 + 60H_2O + NaCl$ system*

244 As with the dimerization in pure water system, four species of silica were identified in this
245 system through following the reaction paths and exploring the PES: orthosilicic acid, OSAZ,
246 $H_3SiO_4^-$, and $H_6Si_2O_7$. Similar to the previous section, only the dimerization reaction of OSAZ is
247 pursued. The calculated paths are shown in table 2.

248 Table 2B and figure 7 show one possible mechanism to dimerization in neutral pH with NaCl
249 present. The process begins with two H_4SiO_4 molecules sitting side-by-side. Next, one of the
250 H_4SiO_4 molecules transforms to OSAZ. Finally, the H_4SiO_4 molecule simultaneously performs a
251 nucleophilic attack on the silicon of OSAZ, transfers a proton via concerted reaction to the
252 OSAZ oxygen, and causes the H_2O group of OSAZ to eject.

253 Figure 8 shows the formation of $H_3SiO_4^-$ from OSAZ. Note that the $H_3SiO_4^-$ species is charge
254 balanced by a distant H_3O^+ formed by concerted transfers from the freed proton (fig. 8J) and is
255 analogous to figure 5F. The energy profiles corresponding to the configurations in figures 7 and
256 8 are shown in figure 9. Neither dipolar complex I nor dipolar complex II was successfully
257 optimized in this system.

258 Although the production of $H_3SiO_4^-$ involved bond breaking and formation between atom centers
259 that were not initially assigned the higher basis set, and no reassignment of atom centers to the

260 higher basis set was deemed necessary. This was decided because the reassignment procedure in
261 the previous section (pure water case) did not significantly modify the reaction direction or the
262 optimized geometries and, therefore, it is surmised that the additional computational effort of
263 altering the atom centers of the basis sets was unnecessary as it would not change the general
264 findings regarding OSAZ reactivity.

265 Computing the molar volumes using the method of Parsons and Ninham (2009) yielded volumes
266 of 1,033 cc/mole and 1,069 cc/mole for figures 7G and 7I respectively, corresponding to NaCl
267 concentrations of 0.967M and 0.935M of NaCl. Likewise, H_4SiO_4 concentrations are double
268 these numbers at 1.934M and 1.870M and are 3 orders of magnitude higher than saturation
269 (1.25×10^{-3}M; Alexander and others, 1954).

270 Similar to the previous section, the thermodynamic results listed in table 3 should not be taken to
271 represent the global thermodynamics of the solution but of the local thermodynamics of the
272 reaction zone. The free energies indicate that the dimerization reaction (eq B1 in table 3) is
273 thermodynamically favored. It is also observed that there is enhancement in the favorability in
274 the formation of OSAZ compared to the pure water case.

275

276 DISCUSSION

277 *The orthosilicic acid zwitterion*

278 Configurationally, OSAZ is what would result if one of the hydrogen atoms from a hydroxide
279 group was moved to another hydroxide in orthosilicic acid resulting in a molecule with an $-O^-$

group and a $-H_2O^+$ group. This is essentially the reaction in figure 2, where the movement of proton occurs through concerted transfers facilitated by surrounding water molecules.

An examination of Lewis formal charges of OSAZ (fig. 2) yields a positive charge on the $-OH_2$ group and a negative charge on the −O group. This doubly charged molecule is the zwitterion state. To confirm the zwitterion characteristics of OSAZ, Hirshfeld and CM5 calculations were conducted on the configurations exhibited in figures 2A and 2B. The results are shown in table 4. Upon transformation to OSAZ, the $-OH_2$ group assumes a positive charge and the -O group takes on a relatively high negative charge.

Note that the magnitude of the charges differs between the Hirshfeld and CM5 results for the $-OH_2$ group. The CM5 method is considered a more reliable estimate than the Hirshfeld method (Marenich and others, 2012) and what is crucial is the direction of change. The sums of the charges are non-zero and slightly negative, whereas the molecule is expected to be neutral. This is likely due to a numerical artifact because the electron density distribution disperses the charges throughout the 90-atom system.

While the recognition of the zwitterion characteristics of OSAZ is new, similar structures have been seen in previous work (Zhou and others, 2002; Mondal and others, 2009). Table 5 compares Si-O bond lengths of these similar structures to the bond lengths in this study.

Orthosilicic acid and OSAZ differ in their intramolecular Si-O bond lengths and O-Si-O bond angles. In general, orthosilicic acid has tetrahedral symmetry having ∠O-Si-O of 109.5º and uniform Si-O bond lengths of 1.630A-1.663A. For OSAZ, the ∠O-Si-O angles are 105.8º for

HO-Si-OH, 103.4º on average for H_2O^+-Si-OH, and 111.8º for H_2O^+-Si-O^-; the bond lengths vary significantly from 1.587A for Si-O^-, 1.653A-1.666A for Si-OH, and 1.715A for Si-OH_2^+.

OSAZ has a superficial resemblance to mono-hydrated metasilicic acid H_2O•($SiO(OH)_2$) with key differences. In OSAZ, four oxygens are covalently bonded around a silicon atom in a distorted tetrahedron, whereas in metasilicic acid, three covalently bonded oxygen atoms are trigonal planar with silicon (Chelikowsky, 1998). Interestingly, metasilicic acid is observed in gas phase ab initio studies, whereas OSAZ-like structures are observed when water molecules are explicitly added to simulations (for example, Mondal and others, 2009; Zhou and others, 2002). Ab initio studies of gas phase metasilicic acid (Mondal and others, 2009) show a H_2O-Si bond that is significantly longer (~1.9A) compared to OSAZ (~1.7A) for OSAZ. These seem to suggest that relaxation of the structure to a more tetrahedral geometry from a trigonal planar one is facilitated by the hydrogen bonds provided by water molecules surrounding the molecule. Furthermore, metasilicic acid is not known to experimentally exist in the aqueous phase, although it has been identified in steam (Hildenbrand and Lau, 1994).

Zwitterion and dipolar complex formation: H_4SiO_4 + 27H_2O +/- NaCl systems

The models in these systems, where a lone H_4SiO_4 interacts with its aqueous environment, are intended to represent silica in dilute concentrations. Hence, the results of the calculations suggest that, in dilute silica concentrations, the zwitterion is more likely to be observed as a stable species where salts are in low concentration while dipolar complex I is more likely to be observed in elevated salt concentrations. This can be interpreted to mean that the polarizing effect of NaCl perturbs the stability of OSAZ and stabilizes the auto-ionization product. (The preference is reversed in environments of higher concentrations of silica, and will be discussed in

the next section.) It should be observed that the formation of OSAZ does not depend on pH (table 1A).

The results predict that the auto-ionization products at 2M NaCl and very dilute silica concentrations is dipolar complex I, where the hydronium ion H_3O^+ sits one water molecule away from the $H_3SiO_4^-$ ion. This configuration is consistently reproducible, for example, in figures 3D and 3D'. The existence of H_3O^+ is corroborated by theoretical (Meraj and Chaudhari, 2014) and empirical studies (Amir and others, 2007; Artemov and others, 2020).

Note that the pK_a of 6.694 for the net reaction in table 1B is much lower than values for the auto-ionization of H_4SiO_4 reported by Sjöberg and others (1981; pK_{a1}=9.472) and similarly by Fleming and Crerar (1982; pK_{a1}=9.687). However, the pK_a value is in close agreement to that derived from amorphous silica titration experiments by von Schindler and Kamber (1968; pK_{a1}=6.8) and near the calculated values of –OH groups on the surface of quartz (Sulpizi and others, 2012; pK_a=5.5). These relationships need further investigation especially since different sites in silica appear to have different acidities (Ostroverkhov and others, 2005; Ong and others, 1992). The dipolar complex may be another silica species in dilute solutions whose concentration is three orders more than the fully ionized $H_3SiO_4^-$. Observe that the pK of the formation of the zwitterion (pK=7.776) is within these ranges and that therefore the concentration of zwitterion is only about one order of magnitude less than dipolar complex I at these concentrations of silica.

The kinetics can be evaluated using transition state theory from the Gibbs free energy of activation, which is related to the rate constant by

$$k = k_B T/h \exp(-\Delta G^{\ddagger}/RT) \qquad (5)$$

where k_B is Boltzmann's constant, R is the gas constant, *T* is the temperature and h is Planck's constant. The rate constants indicate that at the neutral pH regime, dilute silicate concentrations and low salt concentrations, OSAZ is present as an isomer of H_4SiO_4 because equilibration achieves completion in most surface conditions. The rate constant corresponding to the forward reaction equation (A1) in table 1, with a free energy of 56.8 kJ/mol at 298K, is 677 s^{-1} indicating an equilibration time of 1.48 milliseconds. Likewise, the rate constant of the reverse reaction equation (A2) in table 1, with a free energy of 12.5 kJ/mol, is 4.04×10^{10} s^{-1}, indicating and equilibration time of 2.47×10^{-11} seconds. Rate constant calculations for the auto-ionization reactions, equations (B1) and (B2) in table 1, are of similar magnitudes and therefore the reaction completion times are also rapid.

Dimerization by zwitterion: $2H_4SiO_4 + 60H_2O$ (+/-) NaCl systems

The models in these systems, where two H_4SiO_4 molecules are mutually interacting in an aqueous environment, are intended to explore the dimerization reaction, and therefore to investigate energetics of configurations where the local concentration of silica is sufficient to enable encounters between H_4SiO_4 molecules. This scenario can occur at super-saturation, at the water-mineral interface, or during chance encounters due to diffusion. The results of the calculations show that in the presence of a neighboring H_4SiO_4, OSAZ, dipolar complexes, as well as farther separated auto-ionization products, $H_3SiO_4^-$ and H_3O^+, simultaneously occur with or without the presence of NaCl. This is in contrast with the results of the "dilute" system from the previous section where the occurrence of OSAZ is exclusive of the occurrence of dipolar complex I, and vice versa. Another, and more significant, difference is that in the dilute system,

364 auto-ionization is favored over zwitterion formation, whereas the reverse is true in the vicinity of
365 two silica monomers.

366 The dimerization mechanism in this study proceeds differently from previous mechanisms
367 proposed. Instead of forming a chemically reactive nucleophile such as $H_3SiO_4^-$, or forcing two
368 monomers to bond together, the conversion to the zwitterion isomer turns one monomer into a
369 target for nucleophilic attack by a neighboring H_4SiO_4. This mechanism can be more easily
370 extended to oligomerization since it only requires a dangling –OH group from the other reactant
371 (fig. 1). The relative rates between pure water and salt present cases that are expected from their
372 activation energies are in agreement with the observed enhancement of rates with ionic strength.

373 The rate determining step for the neutral pH dimerization process has a zero-point corrected
374 activation energy of 70.7 kJ/mol for the pure water system and 59.8 kJ/mol for the salt-present
375 system (eqns A1 and B2 in table 2), which strongly suggests that the zwitterion pathway is a
376 good candidate for the dimerization mechanism in neutral pH. According to experimental studies
377 (Rothbaum and Rohde, 1979; Makrides and others, 1980), the activation energy for this reaction
378 should be between 12.6 kJ/mol and 71 kJ/mol and therefore, the results of this study are in
379 excellent agreement with experiment. In comparison, the mechanism previously reported by
380 Trinh and others (2006) has an activation energy of 127 kJ/mol for the rate-determining step,
381 while that of Liu and others (2019) has an activation energy of 133 kJ/mol.

382 It might be argued that OSAZ is an insignificant species by virtue of its low concentration upon
383 equilibrium. However, its pH neutrality, its dependence on ionic strength, its dimerization
384 activation energy, and its thermodynamic favorability in the reaction zone all strongly suggest
385 that OSAZ is the key reactive species in the dimerization mechanism and therefore conditions

386 affecting its formation influences the rate of dimerization. Hence, regulating its concentration
387 influences the dimerization mechanism. It is yet to be demonstrated that this can be extended to
388 oligomerization in general.

389 Note that in the pure water case, the occurence of OSAZ is thermodynamically slightly more
390 preferred over $H_3SiO_4^-$ (eqs A3 and A4 in table 3) and this preference is enhanced when NaCl is
391 present (eqs B2 and B3 in table 3). These local thermodynamic preferences are crucial in
392 determining which mechanism predominates because while the slow step in the OSAZ
393 mechanism is the formation of OSAZ itself, the slow step in the next competing mechanism is
394 the attack by $H_3SiO_4^-$ on another monomer (Trinh and others, 2006; Xiao and Lasaga) and is
395 therefore directly dependent on the concentration of $H_3SiO_4^-$. This is why the latter mechanism
396 predominates in higher pH ranges.

397 Equations (A1) and (B1) in table 3 indicate that the dimer is slightly thermodynamically more
398 favored than two monomers. The direction of reaction favorability is similar to Noguera and
399 others (2015) who computed pK_{303}=-0.69. Some workers (Exley and Sjöberg, 2014; Sjöberg and
400 others, 1981) have however implied that the monomer should be slightly more preferred. This
401 deserves further exploration in the future.

402 Comparison with the experimental values of the reverse mechanism, or hydrolysis, is also
403 interesting. The activation energies of the rate-determining step in this study are 126 kJ/mol for
404 the pure water system and 111 kJ/mol for the salt-present system (eqs A6 and B4 in table 2), and
405 are slightly lower than the results of Trinh and others (2006) and Xiao and Lasaga (1994), who
406 got activation energies of 137 kJ/mol and 119 kJ/mol, respectively. However, according to
407 experimental studies (Walther, 1996; Knauss and Wollery, 1988; Brady and Walther, 1990;

Dove and Crerar, 1990), the activation energy for the hydrolysis reaction should be between 67 and 92 kJ/mol, and therefore, the related activation energies in this study (eqs A6 and B4 in table 2) are still too high. Thus, it is for future work to show that the D → [CD]‡ (pure water) step and the I → [HI]‡ (salt-present) step can be broken up into smaller lower activation energy steps.

One intriguing aspect of the simulation is that, although all the points were optimized to local minima and transition states, and while all paths to transition states from their respective local minima yield positive changes in internal energy changes ($\Delta U^{\ddagger}$), the zero-point corrected activation energies ($\Delta U^{\ddagger}_{zpc}$) in equations (A7), (A8) and (A10) in table 2 yield negative values and the Gibbs free energy of activation ($\Delta G^{\ddagger}_{298}$) for equations (A8) and (A10) are also negative. These are likely due to the shallowness of the potential energy wells of the configurations of H_3O^+; it may also be a consequence of the mobility of the proton. However, the true PES is a surface of zero-point corrected points by virtue of the Uncertainty Principle. Therefore, the energy optimized nature of the stationary points in figures 5E, 5F, 5[CE]‡ and 5[EF]‡ need to be approached with caution.

CONCLUSION

The speciation of silica in surface waters is almost universally acknowledged to be predominantly defined by equations (1) and (2), and hence, the recognized main species of monomeric silica are H_4SiO_4, H_3SiO4^- and H_2SiO4^{2-}. The results of this study suggest that there is at least a third reaction that needs to be considered,

$$H_4SiO_4 \leftrightarrow SiO^-(OH)_2(H_2O)^+ \qquad pK=7.7 \qquad (6)$$

429 and that therefore there is a fourth monomeric silica species, $SiO^-(OH)_2(H_2O)^+$ or OSAZ, which
430 is present in solution in amounts significant enough to influence silica chemistry.

431 The kinetic and thermodynamic simulations suggest that the dimerization process in neutral
432 waters is facilitated by this fourth species. In the reaction zone, the formation of OSAZ was
433 found to be energetically more favored than $H_3SiO_4^-$. Thus, it is proposed that the neutral pH
434 dimerization rate depends on the formation of OSAZ, whose concentration is influenced mainly
435 by ionic strength. Only upon the elevation of pH where the concentration of $H_3SiO_4^-$ attains a
436 sufficient level that the basic mechanism takes over.

437

438 ACKNOWLEDGMENTS

439 All computations in this study were performed on Yale high-performance computing servers and
440 the author wishes to thank Mark Gerstein and Yale University for the use of these. The author
441 thanks Prashant Emani and Declan Clarke for proofreading the text and giving invaluable
442 comments. This research did not receive any specific grant from funding agencies in the public,
443 commercial, or not-for-profit sectors.

444

445
446 REFERENCES
447
448 Alexander G. B., Heston W. M., and Iler H. K., 1954, The solubility of amorphous silica in
449 water: Journal of Physical Chemistry, v. 58, no. 6, p. 453–455.
450 Alkorta I., Rozas I., and Elguero J., 2001, Molecular Complexes between Silicon Derivatives and
451 Electron-Rich Groups: Journal of Physical Chemistry A, v. 105, no. 4, p. 743–749.

Amir W., Gallot G., Hache F., Bratos S., Leicknam J., and Vuilleumier R., 2007, Time-resolved observation of the Eigen cation in liquid water: Journal of Chemical Physics, v. 126, p. 034511.

Artemov V. G., Uykur E., Roh S., Pronin A. V., Ouerdane H., and Dressel M., 2020, Revealing excess protons in the infrared spectrum of liquid water: Scientific Reports, v. 10, p. 11320-11329.

Brady P. V., and Walther J. V., 1990, Kinetics of quartz dissolution at low temperatures: Chemical Geology, v. 82, p. 253-264.

Burkett S. L., and Davis, M. E., 1995, Mechanisms of Structure Direction in the Synthesis of Pure-Silica Zeolites. 1. Synthesis of TPA/Si-ZSM-5: Chemistry of Materials, v. 7, p. 1453–1463.

Car R., and Parinello M., 1985, Unified Approach for Molecular Dynamics and Density-Functional Theory: Physical Review Letters, v. 55, p. 2471–2474.

Chelikowsky J. R., 1998, Structural and electronic properties of neutral and charged silicalike clusters: Physical Review B, v. 57, p. 3333-3339.

Cheng X., Chen D., and Liu Y., 2012, Mechanisms of silicon alkoxide hydrolysis-oligomerization reactions, a DFT investigation: ChemPhysChem, v. 13, no. 9, p. 2392-2404.

Criscenti L. J., Kubicki, J. D., and Brantley S. L., 2006, Silicate glass and mineral dissolution, calculated reaction paths and activation energies for hydrolysis of a Q^3 Si by H_3O^+ using ab initio methods: Journal of Physical Chemistry A, v. 110, p. 198-206.

Culkin F., and Cox R. A., 1966, Sodium, potassium, magnesium, calcium and strontium in sea water: Deep-Sea Research, v. 13, p. 789-804.

Cypryk M., and Gostynski B., 2016, Computational benchmark for calculation of silane and siloxane thermochemistry: Journal of Molecular Modeling, v. 22, no. 1, p. 35.

Dove P. M., and Crerar D. A., 1990, Kinetics of quartz dissolution in electrolyte-solutions using a hydrothermal mixed flow reactor: Geochimica et Cosmochimica Acta, v. 54, p. 1267-1281.

Exley C, Sjöberg S., 2014, Silicon species in seawater: Spectrochimica Acta Part A: Molecular and Biomolecular Spectroscopy, v. 117, p. 820-821.

Felipe M. A., Kubicki J. D., and Rye D. M., 2004, Oxygen isotope exchange kinetics between water and dissolved silica from ab initio calculations: Geochimica et Cosmochimica Acta, v. 68, p. 949-958.

Fleming B. A., and Crerar D. A., 1982, Silicic acid ionization and calculation of silica solubility at elevated temperature and pH application to geothermal fluid processing and reinjection: Geothermics, v. II, no. l, p. 15-29.

Frisch M. J., Trucks G. W., Schlegel H. B., Scuseria G. E., Robb M. A., Cheeseman J. R., Scalmani G., Barone V., Petersson G. A., Nakatsuji H., Li X., Caricato M., Marenich A. V., Bloino J., Janesko B.G., Gomperts R., Mennucci B., Hratchian H. P., Ortiz J. V., Izmaylov A. F., Sonnenberg J. L., Williams-Young D., Ding F., Lipparini F., Egidi F., Goings J., Peng B., Petrone A., Henderson T., Ranasinghe D., Zakrzewski V. G., Gao J., Rega N., Zheng G., Liang W., Hada M., Ehara M., Toyota K., Fukuda R., Hasegawa J., Ishida M., Nakajima T.,

Honda Y., Kitao O., Nakai H., Vreven T., Throssell K., Montgomery J. A. Jr., Peralta J. E., Ogliaro F., Bearpark M. J., Heyd J. J., Brothers E. N., Kudin K. N., Staroverov V. N., Keith T. A., Kobayashi R., Normand J., Raghavachari K., Rendell A. P., Burant J. C., Iyengar S. S., Tomasi J., Cossi M., Millam J. M., Klene M., Adamo C., Cammi R., Ochterski J. W., Martin R. L., Morokuma K., Farkas O., Foresman J. B., and Fox D.J., 2019, Gaussian 16, Revision C.01: Gaussian, Inc., Wallingford CT

Gorrepati E. A., Wongthahan P, Raha S., and Fogler H. S., 2010, Silica precipitation in acidic solutions: Mechanism, pH effect, and salt effect: Langmuir, v. 26, no. 13, p. 10467-10474.

Goto K., 1956, Effect of pH on polymerization of silicic acid: Journal of Physical Chemistry, v. 60, no. 7, p. 1007-1008.

van Grotthuss C. J. T., 1806,. Sur la décomposition de l'eau et des corps qu'elle tient en dissolution à l'aide de l'électricité galvanique: Annales de Chimie, v. 58, p. 54–73.

Harrison C. C., and Loton N., 1995, Novel routes to designer silicas: studies of the decomposition of $(M^+)_2[Si(C_6 H_4O_2)_3]\cdot xH_2O$. Importance of M^+ identity of the kinetics of oligomerisation and the structural characteristics of the silicas produced: Journal of the Chemical Society, Faraday Transactions, v. 91, p.4287–4297.

Heenen H. H., Gauthier J. A., Kristoffersen H. H., Ludwig T., and Chan K., 2020, Solvation at metal/water interfaces: An ab initio molecular dynamics benchmark of common computational approaches: Journal of Chemical Physics, v. 152, p. 144703.

Hildenbrand D. L., and Lau K. H., 1994, Thermochemistry of gaseous SiO(OH), $SiO(OH)_2$, and SiO_2: Journal of Chemical Physics, v. 101, p. 6076.

Hirshfeld F. L., 1977, Bonded-atom fragments for describing molecular charge densities: Theoretica Chimimica Acta, v. 44, p. 129–138.

Huˇs M., and Urbic T. J., 2012, Strength of hydrogen bonds of water depends on local environment: Journal of Chemical Physics, v. 136, no. 14, p. 144305.

Hu H., Hou H., He Z., and Wang B., 2013, Theoretical characterizations of the mechanism for the dimerization of monosilicic acid in basic solution: Physical Chemistry Chemical Physics, v. 15, p. 15027-15032.

Icopini G. A., Brantley S. L., and Heaney P. J., 2005, Kinetics of silica oligomerization and nanocolloid formation as a function of pH and Ionic Strength at 25ºC: Geochimica et Cosmochimica Acta, v. 69, p. 293-303.

Iler R. K., 1979, The Chemistry of Silica: Solubility, Polymerization, Colloid and Surface Properties, and Biochemistry: New York, John Wiley and Sons Ltd., 866 p.

Izotova E. D., Rudakova M. A., and Akberova N. I., 2020, The molecular dynamics of silica acids in aqueous solution: Qualitative and quantitative characteristics of oligomers: Uchenye Zapiski Kazanskogo Universiteta. Seriya Fiziko-Matematicheskie Nauki, v. 162, no. 1, p. 5–26.

Kabsch W., 1976, A solution for the best rotation to relate two sets of vectors: Acta Crystallographica, v. A32, p. 922-923.

Kirk S. R., Yin D., Persson M., Carlen J., and Jenkins S., 2011, Molecular dynamics simulations of the aggregation of nanocolloidal amorphous silica monomers and dimers: Procedia Engineering, v. 18, p. 188-193.

Knauss K., and Wolery T., 1988, The dissolution kinetics of quartz as a function of pH and time at 70 ° C: Geochimica Cosmochimica Acta, v. 52, p. 43-53.

Jorge M., Gomes J. R. B., Natália M., Cordeiro D. S., and Seaton N. A., 2009, Molecular dynamics simulation of the early stages of the synthesis of periodic mesoporous silica: Journal of Physical Chemistry B, v. 113, no. 3, p. 708-18.

Liu X., Liu C., and Meng C., 2019, Oligomerization of silicic acids in neutral aqueous solution: a first-principles investigation: International Journal of Molecular Sciences, v. 20, no. 12, p. 3037.

Makrides A. C., Turner M., and Slaughter J., 1980, Condensation of silica from supersaturated silicic acid solutions: Journal of Colloid and Interface Science, v. 73, no. 2, p. 345-367.

Malani A., Auerbach S. M., and Monson P. A., 2010, Probing the mechanism of silica polymerization at ambient temperatures using Monte Carlo Simulations: Journal of Physical Chemistry Letters, v. 1, no. 21, p. 3219-3224.

Martin P., Gaitero J. J., Dolado J. S., and Manzano H., 2021, New kinetic Monte Carlo model to study the dissolution of quartz: ACS Earth Space Chemistry, v. 5, no. 3, p. 516-524.

Mondal B., Ghosh D., and Das A. K., 2009, Thermochemistry for silicic acid formation reaction: Prediction of new reaction pathway: Chemical Physics Letters, v. 478, no. 4, p. 115-119.

Mora-Fonz M. J., Catlow C. R. A., and Lewis D. W., 2007, Modeling aqueous silica chemistry in alkali media: Journal of Physical Chemistry C, v. 111, no. 49, p. 18155-18158.

Mulliken R. S., 1955, Electronic population analysis on LCAO–MO molecular wave functions. I: Journal of Chemical Physics, v. 23, p. 1833–1840.

Noguera C., Fritz B., and Clément A., 2015, Precipitation mechanism of amorphous silica nanoparticles: A simulation approach: Journal of Colloid and Interface Science, v. 448, p. 553-563.

Ong S., Zhao X., and Eisenthal K. B., 1992, Polarization of water molecules at a charged interface: second harmonic studies of the silica/water interface: Chemical Physics Letters, v. 191, p. 327-335.

Ostroverkhov V., Waychunas G. A., and Shen Y. R., 2005, New information on water interfacial structure revealed by phase-sensitive surface spectroscopy: Physical Review Letters, v. 94, no. 4, p. 046102.

Pavlova A., Trinh T. T., van Santen R. A., and Meijer E. J., 2013, Clarifying the role of sodium in the silica oligomerization reaction: Physical Chemistry Chemical Physics, v. 15, no. 4, p. 1123-1129.

Pelmenschikov A.G., Morosi G., and Gamba A., 1997, Adsorption of water and methanol on silica hydroxyls: Ab initio energy and frequency calculations: Journal of Physical Chemistry A, v. 101, p. 1178-1187.

Rimstidt J. D., and Barnes H. L., 1980, The kinetics of silica-water reactions: Geochimica et Cosmochimica Acta, v. 44, p. 1683-1699.

Rimstidt J. D., 2015, Rate equations for sodium catalyzed quartz dissolution: Geochimica et Cosmochimica Acta, v. 167, p. 195–204.

Rothbaum H. P., and Rohde A. G., 1979, Kinetics of silica polymerization and deposition from dilute solutions between 5 and 180°C: Journal of Colloid and Interface Science, v. 71, no. 3, p. 533-559.

von Schindler P., and Kamber H. R., 1968, Die acidität von silanolgruppen: Helvetica Chimica Acta, v. 51, p. 1781-1786.

Sjöberg S., Nordin A., and Ingri N., 1981, Equilibrium and structural studies of silicon(IV) and aluminium(III) in aqueous solution. II. Formation constants for the monosilicate ions $SiO(OH)_3^-$ and $SiO_2(OH)_{22}^-$. A precision study at 25°C in a simplified seawater medium: Marine Chemistry, v. 10, no. 6, p. 521-532.

Sulpizi M., Gaigeot M., and Sprik M., 2012, The silica–water interface: how the silanols determine the surface acidity and modulate the water properties: Journal of Chemical Theory and Computing, v. 8, no. 3, p. 1037–1047.

Tossel J., 2005, Theoretical study on the dimerization of $Si(OH)_4$ in aqueous solution and its dependence on temperature and dielectric constant: Geochimica et Cosmochimica Acta, v. 69, no. 2, p. 283–291.

Trinh T. T., Jansen A. P. J., van Santen R. A., and Jan Meijer E., 2009, The role of water in silicate oligomerization reaction: Physical Chemistry Chemical Physics, v. 11, no. 25, p. 5092-5099.

Trinh T. T., Jansen A. P. J., and van Santen R. A., 2006, Mechanism of oligomerization reactions of silica: Journal of Physical Chemistry B, v. 110, p. 23099-23106.

Walther J. V., 1996, Relation between rates of aluminosilicate mineral dissolution, pH, temperature, and surface charge: American Journal of Science, v. 296, p. 693-728.

Wiberg K. B., and Rablen P. R., 2018, Atomic Charges: Journal of Organic Chemistry, v. 83, no. 24, p. 15463-15469.

Xiao Y. T., and Lasaga A. C., 1996, Ab initio quantum mechanical studies of the kinetics and mechanisms of quartz dissolution: OH^- catalysis: Geochimica et Cosmochimica Acta, v. 60, p. 2283-2295.

Xiao Y. T., and Lasaga A. C., 1994, Ab-initio quantum-mechanical studies of the kinetics and mechanisms of silicate dissolution - $H^+(H_3O^+)$ catalysis: Geochimica et Cosmochimica Acta, v. 58, p. 5379-5400.

Yang Y., Weaver M. N., and Merz K. M. Jr. 2009 Assessment of the "6-31+G** + LANL2DZ" mixed basis set coupled with density functional theory methods and the effective core potential: prediction of heats of formation and ionization potentials for first-row-transition-metal complexes: Journal of Physical Chemistry A, v. 113, no. 36, p. 9843–9851

Zhang J., Zhang H., Wu T., Wang Q., and van der Spoel D., 2017, Comparison of implicit and explicit solvent models for the calculation of solvation free energy in organic solvents: Journal of Chemical Theory and Computing, v. 13, no. 3, p. 1034-1043.

Zhou M., Zhang L., Lu H., Shao L., and Chen M., 2002,. Reaction of silicon dioxide with water: A matrix isolation infrared and density functional theoretical study: Journal of Molecular Structure, v. 605, p. 249–254.

Zhang X., van Santen R. A., and Jansen A. P. J., 2012, Kinetic Monte Carlo modeling of silicate oligomerization and early gelation: Physical Chemistry Chemical Physics, v. 14, no. 34, p. 11969-11973.

TABLES

	ΔU	ΔU_{zpc}	ΔG_{298}	pK_{298}
A. pure water: H_4SiO_4 + 27H_2O system				
Elementary reactions:				
(1) H_4SiO_4 (A) → [AB]‡	59.2	46.4	56.8	
(2) $SiO^-(OH)_2(H_2O)^+$ (B) → [AB]‡	16.2	8.39	12.5	
Net reaction:				
$H_4SiO_4 \leftrightarrow SiO^-(OH)_2(H_2O)^+$	43.0	38.0	44.4	7.78
B. salt present: H_4SiO_4 + 27H_2O + NaCl system				
Elementary reactions:				
(1) H_4SiO_4 (C) → [CD]‡	31.3	23.4	41.8	
(2) H_3O^+•H_2O•$H_3SiO_4^-$ (D) → [CD]‡	5.64	-4.55	3.63	
(3) H_3O^+•H_2O•$H_3SiO_4^-$ (D') → [DD']‡	39.3	24.5	20.6	
Net reaction:				
$H_4SiO_4 \leftrightarrow H_3O^+$•$H_2O$•$H_3SiO_4^-$	25.6	28.0	38.2	6.69

Table 1. Energies for elementary reactions and net reaction. Units are kJ/mol. All are computed in the B3LYP/6-311++G(d,p) level. The dot (•) signifies hydrogen bonding. Elementary reaction energy changes are pseudo-thermodynamic and are denoted by a double-dagger superscript ‡ (e.g. $\Delta U^{\ddagger}$).

	$\Delta U^{\ddagger}$	$\Delta U^{\ddagger}_{zpc}$	$\Delta G^{\ddagger}_{298}$	
A. pure water $2H_4SiO_4 + 60H_2O$				
Elementary reactions:				
(1) $2H_4SiO_4$ (A) → [AB]‡	90.6	70.7	73.1	
(2) $SiO^-(OH)_2(H_2O)^+ + H_4SiO_4$ (B) → [AB]‡	22.9	7.30	7.95	
(3) $SiO^-(OH)_2(H_2O)^+ + H_4SiO_4$ (B) → [BC]‡	19.1	18.7	24.5	
(4) $SiO^-(OH)_2(H_2O)^+ \bullet H_4SiO_4$ (C) → [BC]‡	5.91	11.2	16.6	
(5) $SiO^-(OH)_2(H_2O)^+ \bullet H_4SiO_4$ (C) → [CD]‡	40.4	44.6	49.6	
(6) $H_6Si_2O_7$ (D) → [CD]‡	131	126	134	
(7) $SiO^-(OH)_2(H_2O)^+ \bullet H_4SiO_4$ (C) → [CE]‡	0.811	-2.50	0.785	
	0.358	-2.70	0.438	*
(8) $H_3O^+ \bullet H_3SiO_4^- \bullet H_4SiO_4$ (E) → [CE]‡	0.328	-3.92	-2.31	
	0.875	-4.21	-3.15	*
(9) $H_3O^+ \bullet H_3SiO_4^- \bullet H_4SiO_4$ (E) → [EF]‡	29.7	21.9	24.9	
	28.5	19.3	21.7	*
(10) $H_3O^+ + H_3SiO_4^- \bullet H_4SiO_4$ (F) → [EF]‡	0.806	-5.73	-3.81	
	1.41	-6.43	-4.44	*
B. salt present: $2H_4SiO_4 + 60H_2O + NaCl$				
Elementary reactions:				
(1) $2H_4SiO_4$ (G) → [GH]‡	76.2	59.7	63.8	
(2) $SiO^-(OH)_2(H_2O)^+ + H_4SiO_4$ (H) → [GH]‡	22.8	12.0	13.9	
(3) $SiO^-(OH)_2(H_2O)^+ + H_4SiO_4$ (H) → [HI]‡	42.3	50.1	61.2	
(4) $H_6Si_2O_7$ (I) → [HI]‡	107	111	124	
(5) $SiO^-(OH)_2(H_2O)^+ + 2H_2O$ (H) → [HJ]‡	32.7	27.3	34.1	
(6) $H_3O^+ + H_3SiO_4^-$ (J) → [HJ]‡	28.8	19.2	20.8	

Table 2. Energies for elementary reactions. Units are kJ/mol. All are computed with the B3LYP method and a custom basis set from a combination of 6-311++G(d,p) and 6-31+G(d) basis sets. The dot (•) signifies hydrogen bonding. The asterisk '*' indicates recalculation in a new basis set with a reassignment on atom centers.

	ΔU	ΔU_{zpc}	ΔG_{298}	pK_{298}
A. pure water: $2H_4SiO_4 + 60H_2O$				
Net reactions:				
(1) $2H_4SiO_4$ (A) $\leftrightarrow H_6Si_2O_7 + H_2O$ (D)	-9.54	-10.7	-11.9	-2.09
(2) $2H_4SiO_4$ (A) $\leftrightarrow SiO^-(OH)_2(H_2O)^+ + H_4SiO_4$ (B)	67.7	63.4	65.1	11.4
(3) $2H_4SiO_4$ (A) $\leftrightarrow SiO^-(OH)_2(H_2O)^+ \bullet H_4SiO_4$ (C)	80.8	70.8	73.0	12.8
(4) $2H_4SiO_4$ (A) $\leftrightarrow H_3O^+ \bullet H_3SiO_4^- \bullet H_4SiO_4$ (E)	77.5	69.0	73.3	12.8
(5) $2H_4SiO_4$ (A) $\leftrightarrow H_3O^+ + H_3SiO_4^- \bullet H_4SiO_4$ (F)	106	96.7	102	17.9
B. salt present: $2H_4SiO_4 + 60H_2O + NaCl$				
Net reaction:				
(1) $2H_4SiO_4$ (G) $\leftrightarrow H_6Si_2O_7 + H_2O$ (I)	-11.6	-13.1	-12.8	-2.25
(2) $2H_4SiO_4$ (G) $\leftrightarrow SiO^-(OH)_2(H_2O)^+ + H_4SiO_4$ (H)	53.4	47.7	49.8	8.73
(3) $2H_4SiO_4$ (G) $\leftrightarrow H_3O^+ + H_3SiO_4^- + H_4SiO_4$ (J)	57.3	55.8	63.2	11.1

Table 3. Energies for net reactions. Units are kJ/mol. All are computed with the B3LYP method and a custom basis set from a combination of 6-311++G(d,p) and 6-31+G(d) basis sets. The dot (•) signifies hydrogen bonding.

	Orthosilicic Acid:			Orthosilicic Acid Zwitterion:		
Center	Group	Hirshfeld	CM5	Group	Hirshfeld	CM5
Si	=Si=	0.5414	0.4921	=Si=	0.5095	0.4629
O	-OH	-0.1595	-0.1443	$-O^-$	-0.3679	-0.4599
O	-OH	-0.1505	-0.1479	$-OH_2^+$	0.05479	0.1868
O	-OH	-0.1457	-0.1377	-OH	-0.1488	-0.1431
O	-OH	-0.1475	-0.1421	-OH	-0.1423	-0.1405

Table 4 Charges on atom centers of orthosilicic acid and OSAZ in the pure water system from Hirshfeld population analysis and charge model 5. (Hirshfeld, 1977; Wiberg and Rablen, 2018) Hydrogen charges are summed into the oxygen atoms. Units are atomic units.

H_2O–Si	Si-OH	Reference
1.978	1.653	Zhou et al. (2002)
1.986	1.633-1.651	Mondal et al. (2009)
1.715/1.758	1.653-1.666	This study

Table 5. Bond lengths of OSAZ compared to similar structures in previous studies. Units are in atomic units.

Figure 1. Proposed dimerization reaction and the analogous generalized oligomerization reaction.

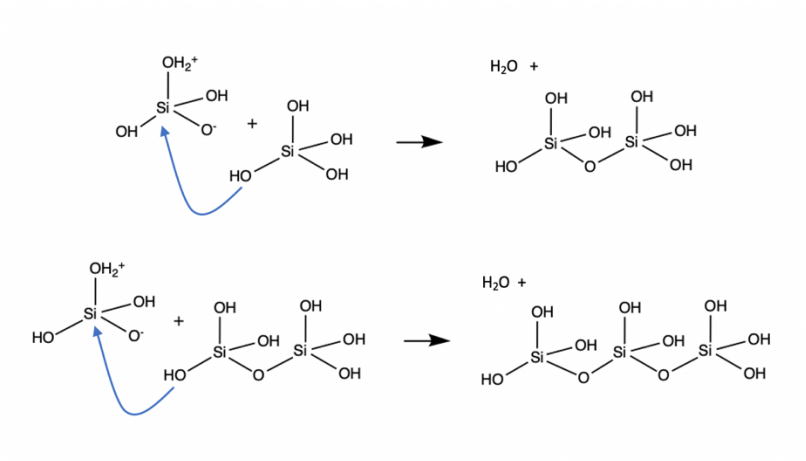

Figure 2. OSAZ formation. Pure water mechanism from orthosilicic acid (A) to OSAZ (B) optimized at the B3LYP/6-311++G(d,p) level. The corresponding energy changes are shown in Table 1.

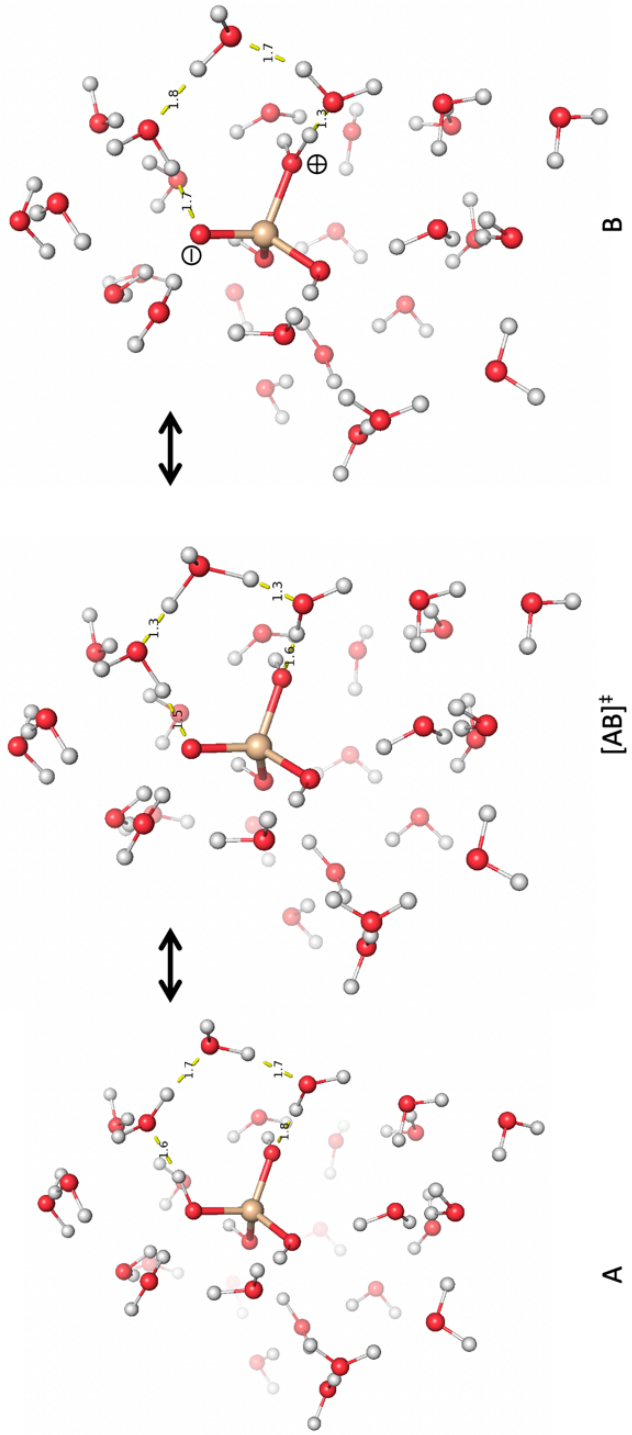

Figure 3. Auto-ionization. Salt present mechanism from orthosilicic acid (C) to its auto-ionization products (D and D') optimized at the B3LYP/6-311++G(d,p) level. The corresponding energy changes are shown in Table 1.

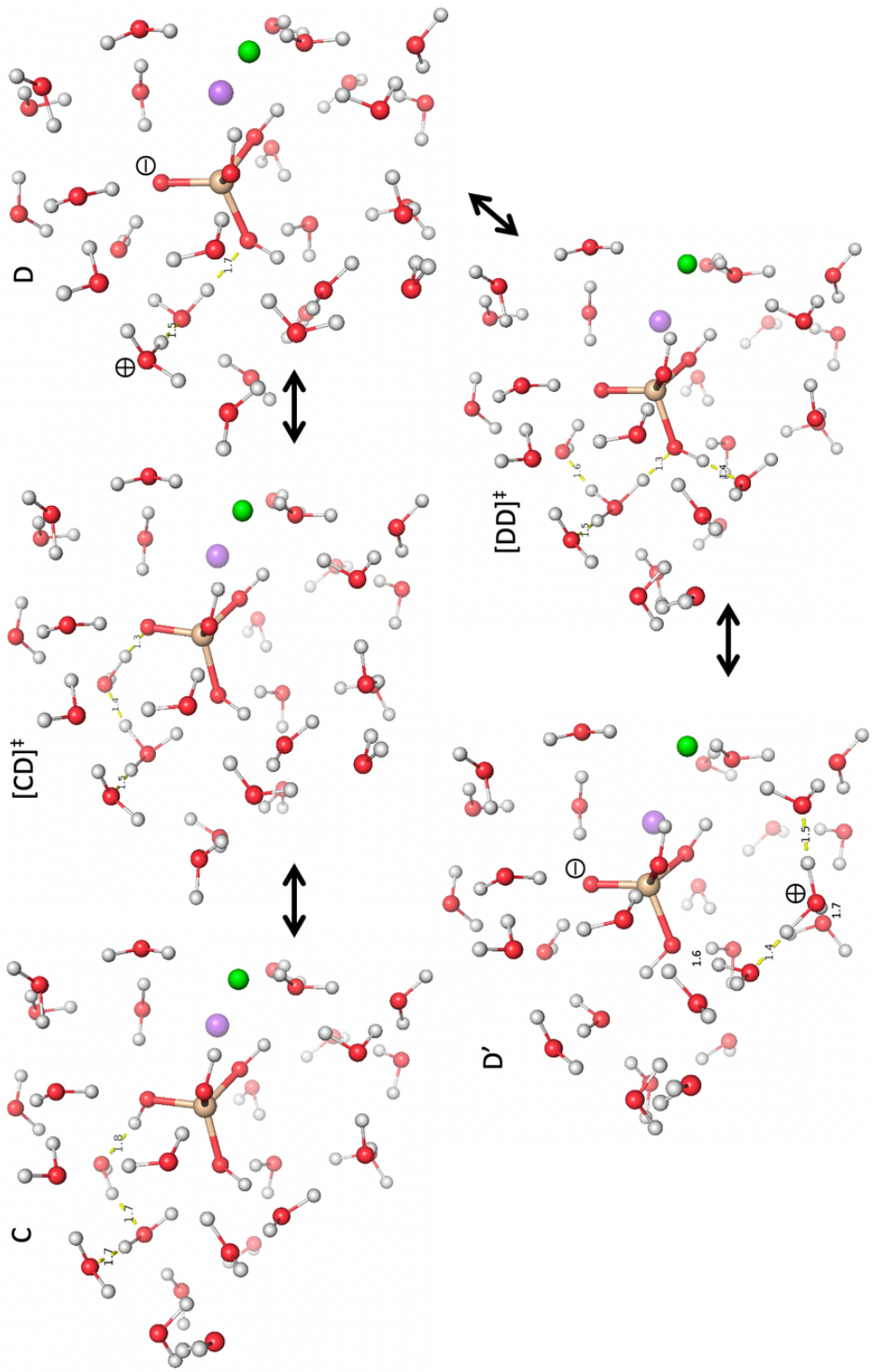

Figure 4. Dimerization in pure water. Mechanism from orthosilicic acid (A) to the dimer (D) optimized with the B3LYP method with customized basis sets. Atoms depicted by ball-and-stick are centers that use the higher level 6-311++G(d,p) basis sets. The rest of the atom centers use 6-31+G(d) basis sets. Corresponding energy changes are shown in Table 2.

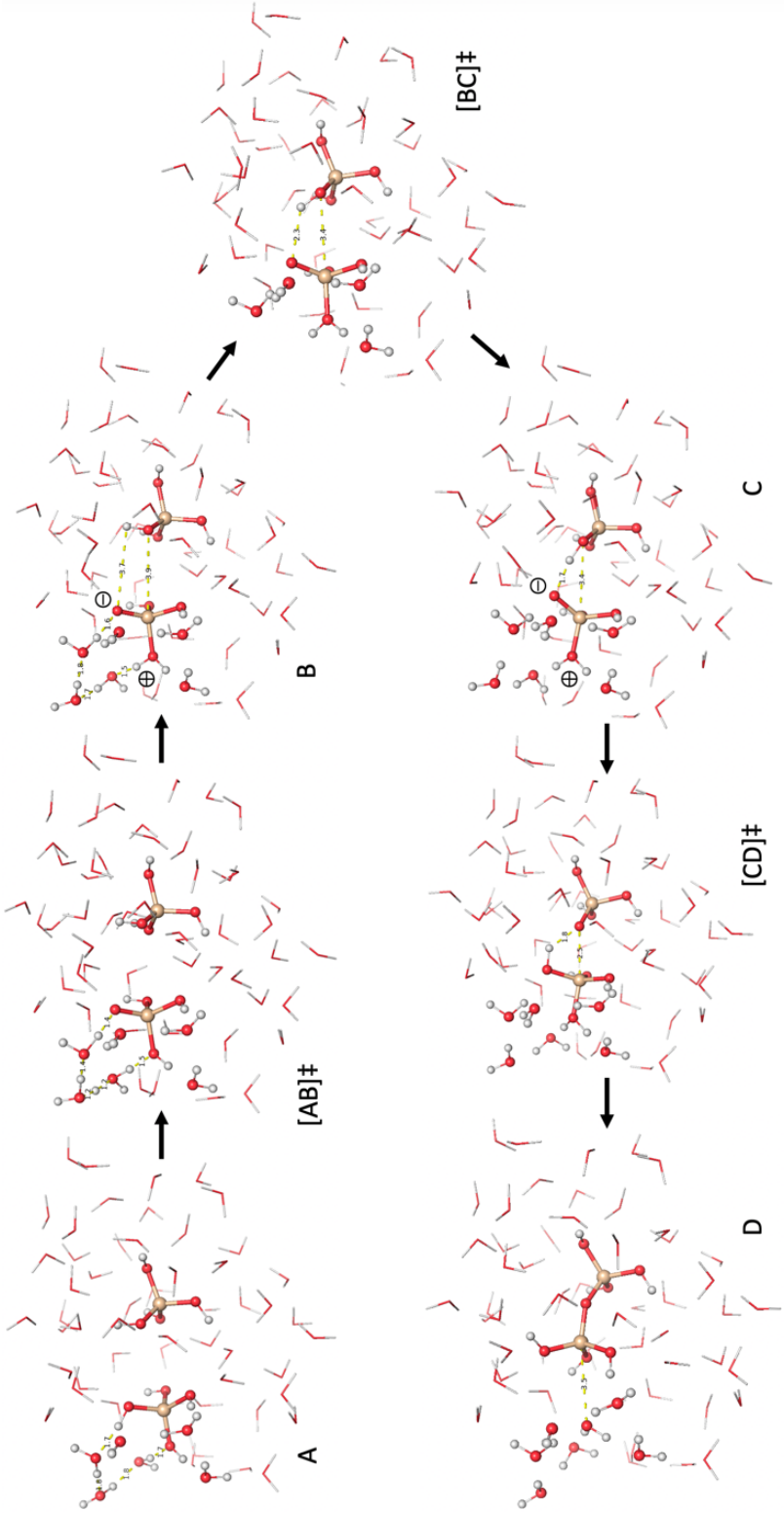

Figure 5. Auto-ionization in pure water. Mechanism from OSAZ (C) to $H_3SiO_4^- + H_3O^+$ (D) optimized with the B3LYP method. Atoms depicted by ball-and-stick are centers that use the higher level 6-311++G(d,p) basis sets. The rest of the atom centers use 6-31+G(d) basis sets. Corresponding energy changes are shown in Table 2.

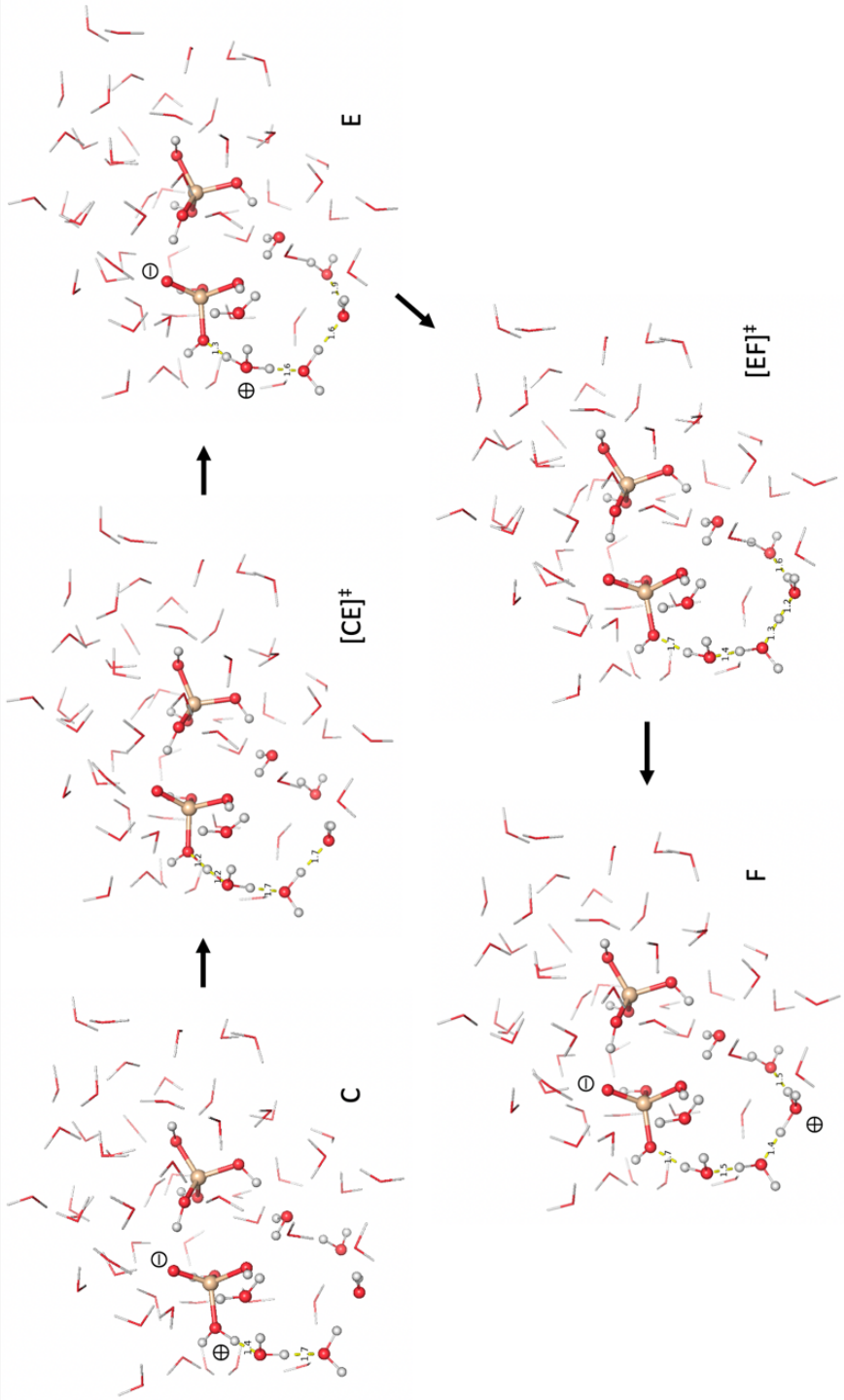

Figure 6. PES Diagram. The letters correspond to configurations in Figure 4 and 5. Energies are in kJ/mol. Solid lines are for uncorrected internal energies and dashed lines are for zero point corrected internal energies. The blue curve corresponds to a recalculation with different atom centers for the higher level basis set. All energies are referenced to the internal energy of configuration A.

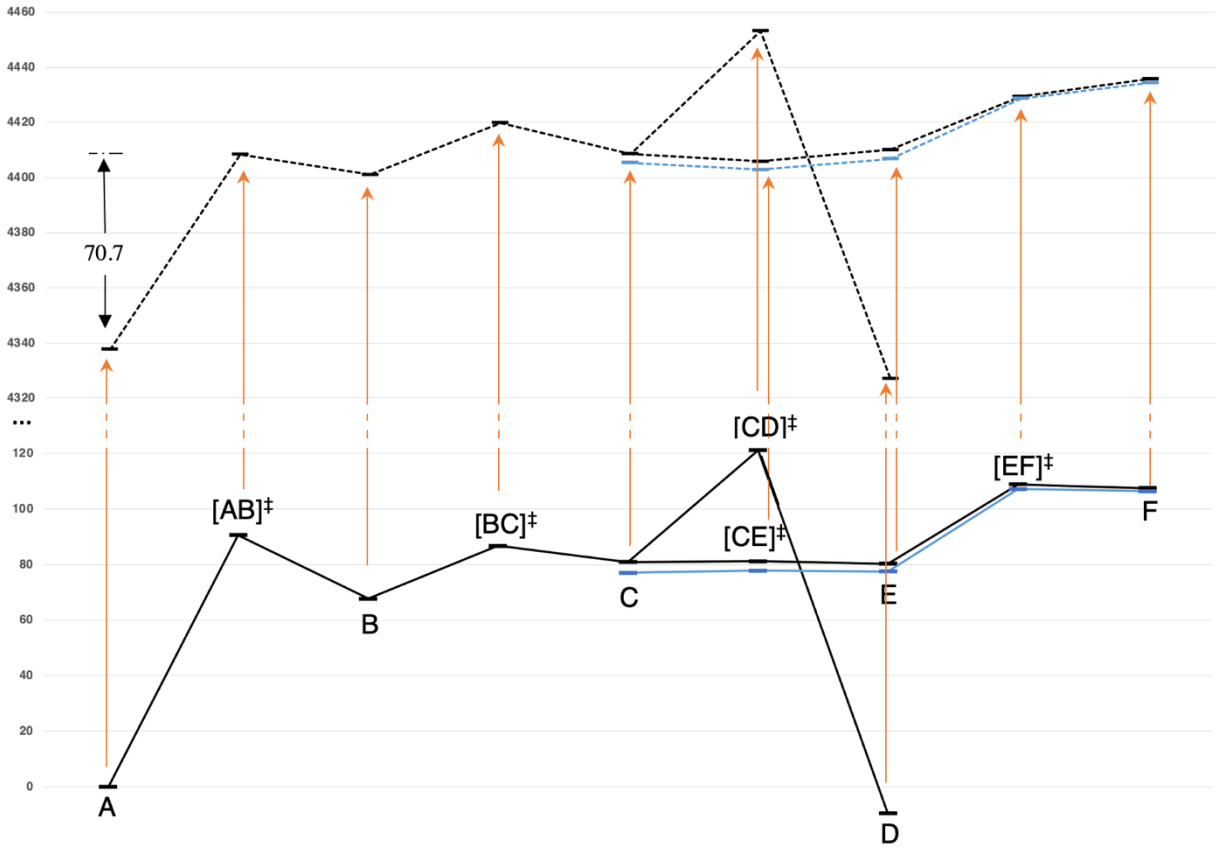

Figure 7. Dimerization with salt present. Mechanism from orthosilicic acid (G) to the dimer (I) optimized with the B3LYP method with customized basis sets. Atoms depicted by ball-and-stick are centers that use the higher level 6-311++G(d,p) basis sets. The rest of the atom centers use 6-31+G(d) basis sets. Corresponding energy changes are shown in Table 4.

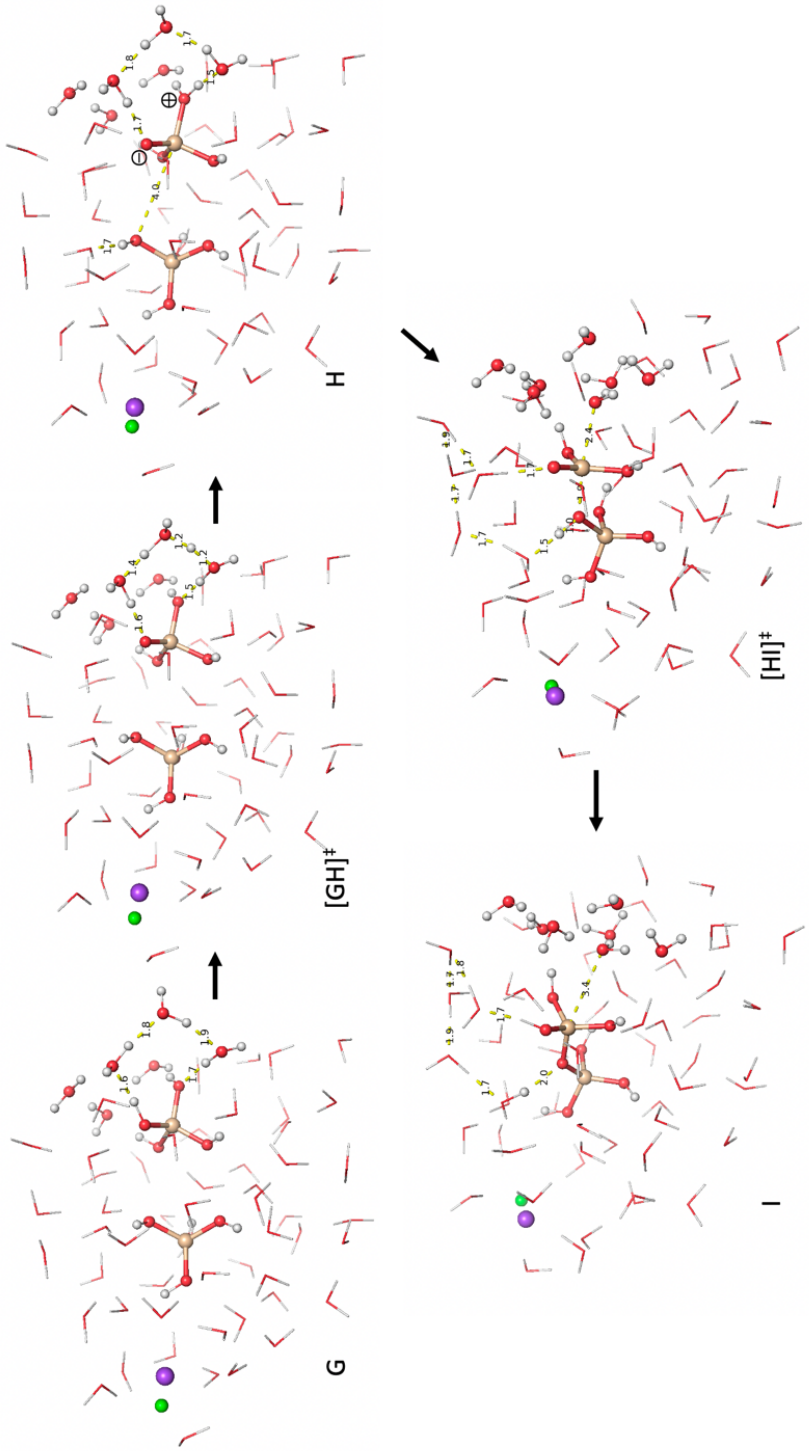

Figure 8. Auto-ionization with salt present. Mechanism from OSAZ (H) to $H_3SiO_4^- + H_3O^+$ (J) optimized with the B3LYP method. Atoms depicted by ball-and-stick are centers that use the higher level 6-311++G(d,p) basis sets. The rest of the atom centers use 6-31+G(d) basis sets. Corresponding energy changes are shown in Table 4.

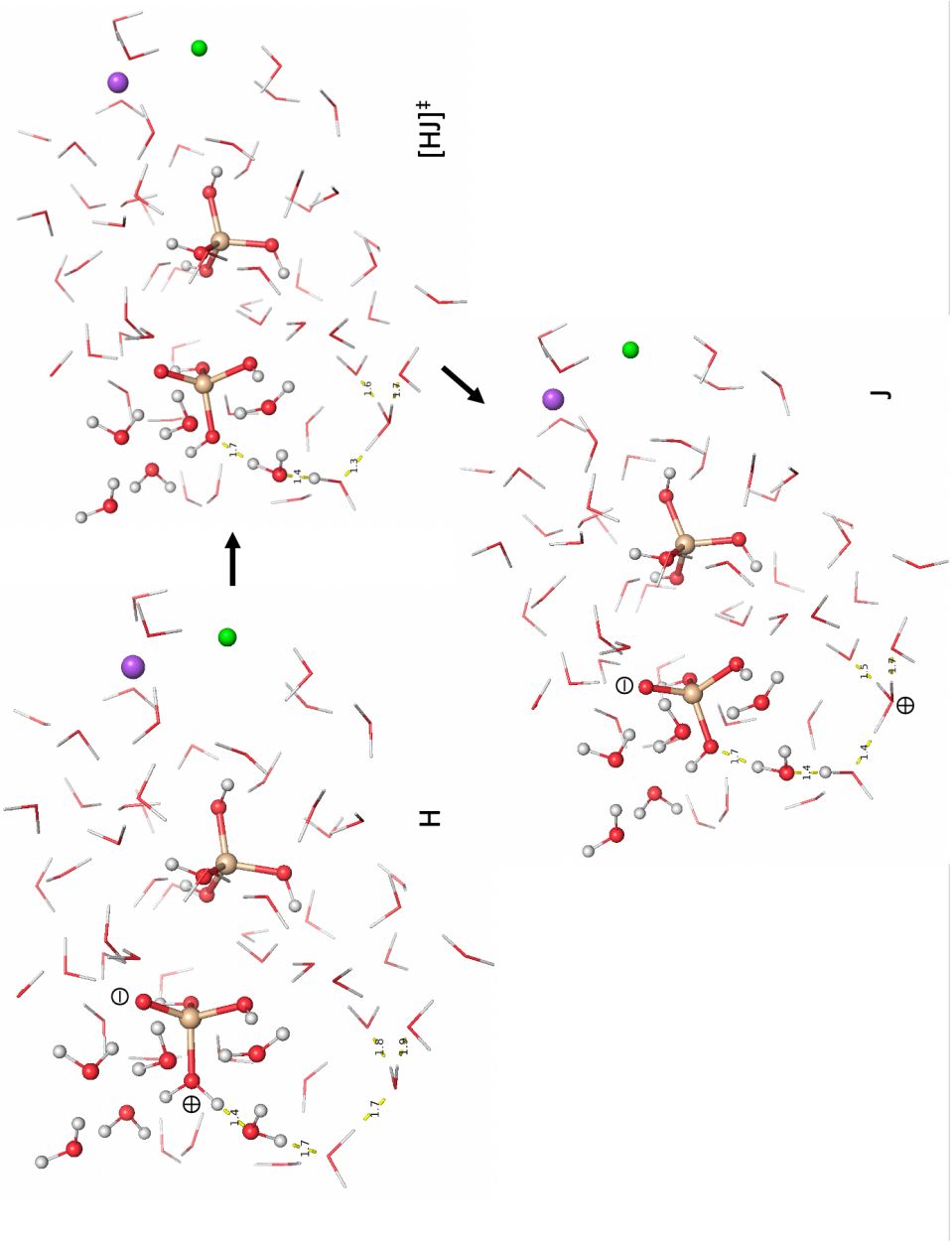

Figure 9. PES Diagram. The letters correspond to configurations in Figure 7 and 8. Energies are in kJ/mol. Solid lines are for uncorrected internal energies and dashed lines are for zero point corrected internal energies. All energies are referenced to the internal energy of configuration G.